Vibrational Resonances and Cu_B Displacement Controlled by Proton Motion in Cytochrome *c* Oxidase

Vangelis Daskalakis,*,† Stavros C. Farantos,†,‡ Victor Guallar,§ and Constantinos Varotsis‡,||

Institute of Electronic Structure and Laser, Foundation for Research and Technology - Hellas, P.O. Box 1527, 711 10 Heraklion, Greece, Department of Chemistry, University of Crete, P.O. Box 2208, 71003, Heraklion, Greece, Barcelona Supercomputing Center (BSC), Centro Nacional de Supercomputación & Institució Catalana de Recerca i Estudis Avançats (ICREA), and Department of Environmental Management, Cyprus University of Technology, P.O. Box 50329, 3603 Lemesos, Cyprus

Received: October 19, 2009

Cytochrome *c* oxidase (CcO), found in the inner mitochondrial membranes or in many bacteria, catalyzes the four-electron reduction of molecular oxygen to water. Four protons are pumped across the inner mitochondrial membrane through CcO. In this study, quantum mechanics/molecular mechanics and molecular dynamics calculations are used to probe the spectroscopic characteristics of the ferryl intermediates in the aa_3 CcO/O_2 reaction. These highly elaborate calculations, supported by several calculations on smaller model systems, demonstrate the sensitivity of vibrational frequencies on the Coulombic field of heme a_3 and their dependence on the distance of the adjacent Cu_B to the heme a_3-Fe atom. This distance seems to be associated with the protonation state of the heme a_3 propionate A, and we propose that it plays a crucial role on the mechanism of action of CcO. In detail, we link proton pumping activity in CcO enzyme (a) to a multiple (1:1:2) resonance among the frequencies of Fe^{IV}═O bond stretching, the breathing mode of Histidine 411, and a bending mode of the His411-Fe^{IV}═O species (aa_3 from *Paracoccus denitrificans* numbering) and (b) to Cu_B displacement by electrostatic interactions toward the heme a_3 iron. We find that the vibrations of the His411-Fe^{IV}═O unit become highly coupled depending on the protonation state of the heme a_3 ring A propionate/Asp399 pair, and we propose a mechanism for the resonance Raman enhancement of the bending mode δ(His411-Fe^{IV}═O). Calculations on model systems demonstrate that the position of Cu_B in relation to heme a_3 iron-oxo plays a crucial role in regulating that resonance. We also discuss the origin of the coupling between bending, δ(His411-Fe^{IV}═O) and ν(Fe═O) stretching modes, and the role played by such vibrational coupling interactions or Cu_B position in controlling functional properties of the enzyme, including electron/proton coupling as well as experimental spectra.

I. Introduction

Cytochrome *c* oxidase (CcO), found in the inner mitochondrial membranes or in many bacteria, catalyzes the four-electron reduction of molecular oxygen to water, as part of the process called oxidative phosphorylation. Four protons are pumped across the inner mitochondrial membrane, by CcO, attributing to the electrochemical gradient needed for the phosporylation of ADP to ATP by ATP-synthase.[1] The crystal structure analysis reveals, for the active site of CcO, where oxygen is bound and reduced: (a) a Cu_B complex with the metal being coordinated to three Histidine residues and (b) a heme-Fe site with the fifth axial ligand being the so-called proximal Histidine.[2−5] The active site of aa_3 CcO from *Paracoccus denitrificans* is depicted in Figure 1.[3] In this crystal structure, the heme a_3 propionate-A side chain forms hydrogen bonding interactions with Asp399 and His403 residues. For reviews on the function and proposed mechanisms of action of CcO enzymes, see refs 6−9. The O−O bond scission produces the ferryl-oxo (heme-Fe^{IV}═O /Cu_B^{II}) species.[10,11] We have recently reported,[12] on a theoretical level, that the protonation state of the heme-ring−A propionate−Asp399 (prop-A/Asp399) pair affects significantly the Fe═O stretching frequency, ν(Fe═O), in *P. denitrificans*. This way, we have linked ferryl-oxo spectroscopic characteristics to proton pumping activity. The Prop-A/Asp399 pair has been suggested to be involved in proton pumping activity experimentally.[13−15] Absorption spectroscopy coupled with resonance Raman (RR) spectroscopy has been recognized as an excellent tool for direct detection and characterization of the Fe^{IV}═O unit.[7,10] The Fe═O stretching mode appears in the 750−850 cm^{-1} region when laser excitation wavelength is tuned into the Soret maximum absorption band of the His-(Porphyrin)Fe^{IV}═O moiety.[10,16−18] The enhancement of the Fe^{IV}═O stretching mode in the RR experiments has been proposed to occur through $\pi(a_{2u})\rightarrow\pi^*(d_{xz},d_{yz})$ and $\pi(a_{1u})\rightarrow\pi^*(d_{xz},d_{yz})$ electronic excitations, while the proximal ligand could play a crucial role in tuning Fe^{IV}═O spectroscopic properties.[19] We have demonstrated that the frequency of the Fe^{IV}═O stretching mode is associated with a family of periodic orbits located in the active site of CcO that show high anharmonicity (family f139 in Figure 3 of ref 12); i.e., the frequency deduced from the period of the periodic orbit is rapidly reduced by increasing the energy.

Several details of the mechanism of action of CcO remain yet to be clarified, despite the substantial work that has been performed on both experimental and theoretical levels. An

* Corresponding author. Tel.: +30 2810 545003. Fax: +30 2810 545160. E-mail: vdas@her.forthnet.gr.
† Foundation for Research and Technology - Hellas.
‡ University of Crete.
§ Centro Nacional de Supercomputación & Institució Catalana de Recerca i Estudis Avançats.
|| Cyprus University of Technology.

10.1021/jp910006k
Published on Web 12/04/2009

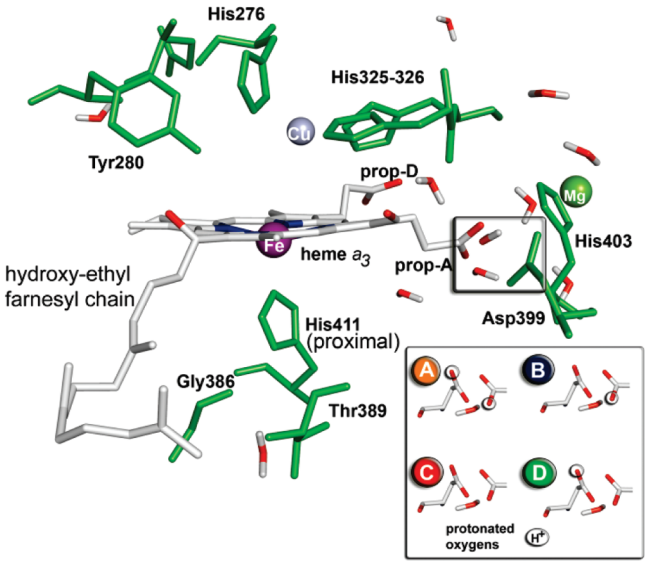

Figure 1. Active site of aa_3 CcO from *Paracoccus denitrificans*, containing roughly 300 atoms. A crucial interaction, via hydrogen bond, of the heme a_3 ring A propionate with Asp399 is also visible. In the inset, different protonation cases of ring A propionate of heme a_3 and Asp399 are shown. (A) Both ring-A propionate and Asp399 protonated. (B) Ring-A propionate deprotonated and Asp399 protonated. (C) Both deprotonated. (D) Ring-A propionate protonated and Asp399 deprotonated.

interesting feature of the RR spectra, which is under considerable debate, is the peak in the 350−360 cm^{-1} region, originally discovered by Ogura et al.[20] and assigned to the δ(His-Fe═O) bending vibration of the ferryl-oxo species.[18] Table 1 summarizes the experimental spectroscopic properties of the oxo-ferryl intermediate, found in the literature,[6,10,16,18,21−25] emphasizing the Fe^{IV}═O stretching and His-Fe^{IV}═O bending modes. As can be observed, vibrational spetra in the 350−810 cm^{-1} region exert different characteristics for ν(Fe═O) and δ(His-Fe═O) modes depending on the reaction scheme and experimental setup, including available electrons in the system and pH dependence. Interestingly enough, the P ferryl species ($2e^-$ reduced) exerts the 356 cm^{-1} bending vibration, whereas the vibrational spectrum of the F ferryl species ($3e^-$ reduced) exerts no such characteristic.[21] As noted before, the origin of the 356 cm^{-1} band has long been under debate.[6,16,22] The proposed assignment of the band at 356 cm^{-1} to the N(His)-Fe═O bending mode[18,22] is also consistent with a theoretical calculation.[26]

The ferryl-oxo species is linked to the proton pumping activity of CcO, but a link between ν(Fe═O) and δ(His-Fe═O) bending vibration to the protonation states or proton pumping activity has not been reported. To gain an understanding of the link between ν(Fe═O) and δ(His-Fe═O) bending vibration with protonation states and/or proton pumping activity of the enzyme, we have constructed four ferryl-oxo protein models based on the crystal structure of the aa_3 oxidase from *P. denitrificans*[3] solvated in water buffer. Four protonation states of the prop-A/Asp399 pair have been prepared, **A** with the pair fully protonated and **C** fully deprotonated, **B** with Asp399 only protonated, and **D** with prop-A protonated, as possible transient species during proton motion and proton pumping activity (see inset of Figure 1). In the present study, we use Quantum Mechanics/Molecular Mechanics (QM/MM) and Molecular Dynamics (MD) methodologies to probe structurally and spectroscopically the above models. QM/MM approaches join together a quantum and a classical representation of different sectors of a complex condensed phase system. The conjunction of these technologies contains the elements necessary to properly describe the electronic properties of enzymatic systems. The reactive region of the active site can be treated with a robust ab initio quantum mechanics methodology. The remainder of the protein can be modeled at the molecular mechanics level, providing the appropriate structural constraints in addition to the electrostatic and van der Waals interactions with the core reactive region.[27]

In this study, we report the theoretical vibrational frequencies associated with the Fe═O stretchings, Imidazole (His411) breathing, and His-Fe═O bending to link spectroscopic characteristics to proton movement during enzymatic turnover in CcO. Cu_B position, in relation to the heme-Fe^{IV}═O unit, changes by the proton pumping activity. In turn, multiple resonances occur between the above three vibrational characteristics, depending on the protonantion state of the prop-A/Asp399 pair. This Cu_B displacement upon protonation/deprotonation events can have direct involvement in the mechanism of action of CcO, coupling proton and electron through pure electrostatic interactions. Moreover, vibrational resonances are significant effects in molecular spectroscopy, and they bring a surprise when they are met in large biomolecules where coherence is sought.

II. Computational Methods

All simulations were carried out with initial Cartesian coordinates from the crystal structure of a two-subunit aa_3 CcO from *Paracoccus denitrificans* (protein databank code 1AR1). Because of its smaller size, this two-subunit CcO protein from *P. denitrificans* serves as an analogue to the aa_3 oxidase from beef heart which has been extensively studied experimentally in ferryl states.[28−33] Subunits I and II show a high degree of homology between these two enzymes coming from different organisms. Protonation states of amino acids like Histidine, Aspartic, and Glutamic were checked visually and corrected when needed to reproduce hydrogen bonding networks or electrostatic interactions with metals like Cu, Fe, Mg, and Ca. A Tyr280-His276 cross-link was added. Residue Glu278, acting as a proton shuttle or valve,[34,35] at the entrance of the D-proton pathway was left protonated. Histidine residues 403, 411, and 325−326 were set protonated at N_δ sites, while His276 was set deprotonated at both N_ε and N_δ sites. The rest of the titratable sites were also checked and compared against the results from the H^{++} online protonation state prediction algorithm of Virginia Tech.[36]

A. QM/MM Methodology. Crystallographic waters inside the protein structure were retained, and an additional box of at least 12 Å distance between protein and its boundaries, full of water molecules, was implemented, yielding a total volume of around 790 000 $Å^3$ and 76 000 atoms, including solvent. For the protein, the OPLS2005[37−39] Force Field (FF) was employed, while for all the solvent molecules TIP3P[40] FF was used. The minimization/relaxation process was performed by Desmond Software of Schrodinger Suite 2008,[41] and it was based on the default proposed protocol.[42] For the QM/MM geometries, we reduced the water buffer significantly by excluding every solvent molecule beyond a distance of 8 Å off the protein matrix and froze those waters beyond a 20 Å layer around the heme a_3 iron to their minimized position. A cutoff distance of 100 Å was also set. All QM/MM calculations were performed with the QSite program.[43] The quantum region included heme a_3 with a truncated hydroxyl-ethyl farnesyl side chain with only three carbon atoms included, proximal Histidine 411, Cu_B coordinated to Histidines 325−326 and 276, as well as the Tyrosine 280

TABLE 1: Various Experimental Vibrational Data on the Oxo-ferryl Species Occurring in the Cytochrome *c* Oxidase + O_2 Reaction[a]

enzymes/reactions	ferryl optical properties (Soret maxima of heme group)	ν(Fe=O) stretching	δ(His-Fe=O) bending
Cu_A^{1+}/Cu_A^{1+}, heme a^{2+}, heme a_3^{2+}-Cu_B^{1+}, fully reduced CcO + O_2	P_R ($2e^-$ reduced) intermediate 607 nm,[24] F ($3e^-$ reduced) intermediate 580 nm	(a) 785−790, 804 cm^{-1}[10,18] or (b) only 790 cm^{-1}[16]	356−360 cm^{-1} for P intermediate (mode not observed in F intermediate)[6,16,18,22]
$Cu_A^{1.5+}/Cu_A^{1.5+}$, heme a^{3+}, heme a_3^{2+}-Cu_B^{1+}, mixed valence CcO + O_2	P_M ($2e^-$ reduced) intermediate 607 nm[24]	804 cm^{-1}[17,21]	356−360 cm^{-1}[16,16,18,21,22]
oxidized CcO + H_2O_2	P ($2e^-$ reduced) intermediate 607 nm	804 cm^{-1}[23−25]	
	F ($3e^-$ reduced) intermediate 580 nm	785−790 cm^{-1}[23−25]	

[a] Emphasis is given in the Fe^{IV}=O stretching and His-Fe^{IV}=O bending modes.

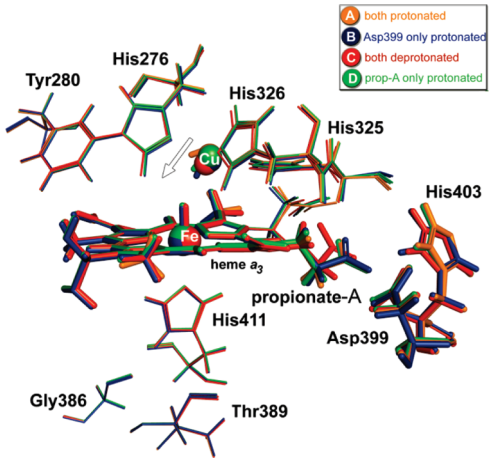

Figure 2. Active site area in QM/MM optimized geometries in an overlapped scheme for different protonation cases of the prop-A/Asp399 pair, emphasizing the propionates and Fe−Cu_B sites. Mulliken Spin population analysis on heme-Fe, Cu_B, oxo-ferryl oxygen, and the hydroxyl group of Cu_B gave the values of 1.30, −0.52, 0.76, and −0.31, respectively, for all the structures, with only negligible deviations. The coloring scheme used is: orange for **A**, blue for **B**, red for **C**, and green for **D** protonation case of the heme a_3 ring A propionate/Asp399 pair. Differences are observed in the prop-A/Asp399 geometry, His403 orientation, and Fe·Cu_B(OH) distance among the diverse conformations. Especially for the **C** structure (red), both prop-A and His403 swing away from the deprotonated Asp399 residue. Fe·Cu_B distances are calculated as follows: **A** (4.26 Å), **B** (4.12 Å), **C** (3.83 Å), and **D** (4.24 Å).

cross-linked to Histidine 276. In addition, Aspartic 399 and Histidine 403 in the region of propionates, as well as Glycine 386 and Threonine 389 in the proximal area, were also included in the QM region containing a total of around 270 atoms (Figure 2). The H-cap approach was used for the covalent QM-MM boundary region. For the QM region, we have used the DFT B3LYP level of theory with the lacvp* basis set for geometry optimizations. The lacvp* basis sets are a combination of the 6-31G* basis set with the lanl2dz effective core basis set. Specifically, the atoms H to Ar are described with the 6-31G* basis set, while heavier atoms are modeled using the lanl2dz basis set (Dunning/Huzinaga valence double-ζ,[44] Los Alamos ECP plus DZ on Na−La, Hf−Bi[45−47]). Consistent with the equilibration relaxation protocol, as well as the MD simulations below, the MM region was described by the OPLS2005 FF.[38,39]

B. MD Methodology. We used initial Cartesian coordinates from the QM/MM protonation state **A** optimized structure and charges fitted to quantum mechanical electrostatic potential (ESP) maps. This structure was solvated and neutralized (adding ions) to the final (871683 $Å^3$) volume and minimized/relaxed with the protocol mentioned above. Fe=O, His411-Fe, Cu_B−OH, and Cu_B-His harmonic bonds were introduced with parameters based on our previously developed force field.[12] Angles, dihedrals, van der Waals, and 1−4 pair interactions were also added, accordingly, to fit the OPLS2005 FF parametrization standards, yielding a simulation box of 81 × 88 × 123 $Å^3$ dimensions with 84 574 atoms, including solvent (described as the TIP3P model[40]). On the basis of this simulation box, a 5 ns run was started in NVT ensemble at energy equivalent to 300 K, with a potential tapering between 14 and 16 Å, a time step of 2 fs, and constraining heavy atom−hydrogen covalent bonds with a tolerance of 10^{-8} Å (8 iterations). Coulombic electrostatic interactions were also taken into account. The RESPA integrator[43] implemented in Desmond was used to integrate the equations of motion. Twenty frames (or intermediate structures) were collected, each one every 250 ps, throughout this 5 ns run. For the protein backbone of α-carbon atoms, C_α, we calculated the rmsd value for every frame in relation to the initial one. This gave a mean rmsd value of 1.31 Å, while for the QM/MM initially minimized/relaxed geometry the rmsd value of around 1.08 Å was calculated in relation to the original pdb structure coded 1AR1.

For each frame collected previously, we run a short 43.5 ps simulation at NVE ensemble, to extract vibrational frequencies. Potential tapering was used between 14 and 16 Å and a time step of 0.5 fs. Throughout the simulation, we collected the Fe=O bond and Fe-His411 and CD2-NE2-CE1 (His411) angle time series. Elongating the Fe=O bond to 1.8, 2.0, 2.2, and 2.5 Å (equilibrium bond length at 1.67 Å), again for every frame, we repeated the 43.5 ps NVE run collecting time series immediately after the perturbation. The simulation time was chosen to be small, to observe the flow of energy around the Fe=O moiety and the excitations induced. Fast Fourier transforming these time series, and averaging over the twenty 43.5 ps long trajectories, gave the power spectra for the corresponding vibrations. In a resonance Raman experiment, the $\pi \rightarrow \pi^*$ excitation on the His-(porphyrin)Fe^{IV}=O system induces also an enhancement for the Fe^{IV}=O stretching, thus making the mode visible on the spectrum. Accordingly in MD, we introduced additional energy at the His-(porphyrin)Fe^{IV}=O system, triggering the initial enhancement of the Fe=O stretching vibrational mode at ∼800 cm^{-1}.

C. DFT Methodology. Truncating QM/MM structures to the level of the active site or only the Fe-heme a_3 site, we perform density functional theory (DFT) calculations at the b3lyp/lacvp* level of theory and subsequent evaluation of the Hessian to calculate vibrational frequencies, using the Jaguar Software of the Schrodinger Suite 2008.[41]

All the frequencies reported in this work refer to vibrations with the strongest Fe=O stretching, Imidazole breathing, or His-Fe=O bending character, while several others exist but with significantly lower or negligible character of the above-mentioned vibrations. When vibrational frequencies are calculated by electronic structure theory, they can be improved by scaling, and it is useful to have general scaling factors. Such

TABLE 2: Theoretical Vibrational Frequencies in the QM/MM Level of Theory for the Protonation Cases A, B, C and D. Comparison between Experiment and Theory is also Included

protonation states	ν(Fe=O) stretching O^{16}/O^{18} in cm^{-1}	δ(His-Fe=O) O^{16}/O^{18} in cm^{-1}
A	738, 802/697, 777	363, 377, 237/352, 362, 229
B	808	368, 376, 241
C	812	370, 378, 240
D	808	370, 377, 241
experiment (refs in Table 1)	785−790, 804	356−360

factors depend on the level of electronic structure theory and the one-electron basis set. It has been established that calculated frequencies may be scaled in various ways.[48] For example, one scaling factor is applied to reproduce the true harmonic frequencies, the true fundamental frequencies, or the zero point energy. To accurately reproduce the experimental ν(Fe=O) at around 800 cm^{-1}, a scaling factor of 0.85 has been applied to QM/MM and DFT level derived frequencies. That lowers the absolute calculated numbers to the experimental ones for stretching and bending. For example, the ν(Fe=O) is lowered from 944−950 (QM/MM) to ∼800 cm^{-1} and δ(His411-Fe=O) from around 430−440 (QM/MM) to ∼360 cm^{-1} (protonation cases **A**, **B**, **C**, and **D**).

III. Results and Discussion

A. QM/MM Calculations. The active site region of each QM/MM **A**, **B**, **C**, and **D** optimized structure is shown in Figure 2 at an overlapping scheme, emphasizing the propionates and the Fe−Cu_B sites. No significant differences can be observed apart from the Fe·Cu_B(OH) position and prop-A/Asp399/His403 site. In the case where the prop-A and Asp399 sites are protonated (conformation **A**, orange), the optimized geometry has Cu_B at the longest distance (4.26 Å) from the heme-Fe, while it is optimized at its shortest one (3.83 Å) when the prop-A/Asp399 pair is fully deprotonated (conformation **C**, red). From a first point of view, the displacement of Cu_B toward the iron-oxo moiety is due to electrostatic effects from the propionate region, with the fully negatively charged area on structure **C** strongly attracting the copper ion toward the heme plane.

Table 2 depicts the theoretical results in this study for the different protonation cases **A**, **B**, **C**, and **D**, as well as a comparison to the experimental data. Evaluation of the Hessian and calculation of the vibrational frequencies at the same level of theory (b3lyp/lacvp* QM/OPLS2005 MM region) shows two vibrations with strong Fe=O stretching character at 738 and 802 cm^{-1} for the **A** case and mainly one with strong Fe=O stretching character for **B**, **C**, and **D** at 808, 812, and 808 cm^{-1}, respectively. The proximal Imidazole (His411) breathing vibration appears at 738 cm^{-1} for **A** and **B** cases and at 740 and 747 cm^{-1} for **C** and **D** cases, respectively. Thus, only in protonation case **A**, ν(Fe=O) seems to be coupled to the Imidazole breathing vibration at 738 cm^{-1}. This can also be deduced by substituting ^{14}N at the proximal His411 by its ^{15}N isotope. While we observe a broadening for the lines at 808, 812, and 808 cm^{-1} for the **B**, **C**, and **D** cases, in the conformation **A** the 802 cm^{-1} disappears and splits into 774, 785, and 795 cm^{-1}, while ν (Fe=O) = 738 cm^{-1} remains unshifted. In Figure 3a we depict a graphical representation of the various vibrational frequencies for Fe=O stretching, proximal Imidazole breathing, and the bending frequency, δ(His411-Fe=O), with the latter multiplied by two. Three main vibrations with His411-Fe^{IV}=O bending character are observed for all cases **A**−**D** for the *P. denitrificans* aa_3 enzyme. Especially for the protonation state **A**, the 363 mode, which satisfies better the 1:2 resonance condition with the ν(Fe=O), includes an out-of-plane heme a_3 character vibration, while the higher one (377 cm^{-1}) exerts a pure His411-Fe^{IV}=O bending character. For the rest of the cases **B**, **C**, and **D**, the vibrational frequencies attributed to δ(His411-Fe=O) appear at (368 and 376 cm^{-1}), (370 and 378 cm^{-1}), and (370 and 377 cm^{-1}), as seen in Figure 3a. Only two vibrational frequencies for the bending are depicted in Figure 3a for clarity.

A QM/MM approach was also applied to the protein models in protonation states **A**, **B**, **C**, and **D**, as described above, but with ^{18}O isotopic substitution of both ferryl-oxygen and the oxygen bound on Cu_B(II). Vibrational frequency analysis reveals interesting behavior. The ν(Fe=O) stretching vibration is again coupled to the Imidazole (His411) breathing vibration at 697 cm^{-1} in the structure **A**, while another ν(Fe=O) peak appears at 777 cm^{-1}. Bending vibrations for the same protonation case exhibit peaks at 352 and 362 cm^{-1}, implying once more the 697:697:2 × 352 (1:1:2) resonance relation. It is in fact intriguing to find such a strong coupling in protonation case **A** that ^{18}O substitution also shifts the proximal Imidazole (His411) breathing vibration observed at 738 cm^{-1} on the ^{16}O model.

B. DFT Calculations on Active Site Small Models. To further investigate the assumption on induced Cu_B movement, by electrostatic effects and the mechanism of the subsequent effect on ν(Fe=O), we constructed three smaller models (**I**, **II**, and **III**) of the active site and optimized at the b3lyp/lacvp* level of theory.

In model **I**, Cu_B is coordinated to three imidazoles and an OH group with the heme iron in the ferryl oxidation state coordinated to an imidazole as the fifth axial ligand and the porphyrin with only the two propionate side chains, with prop-A interacting with truncated His403 and Asp399 residues. Several carbon atoms were retained to their QM/MM optimized coordinates from the QM/MM protein models, to avoid deviation from crystal structure. Copper is again approaching the heme plane as we deprotonate propionate A with the Fe−Cu_B shifting from 3.83 to 3.72 Å.

In model **II**, Cu_B is coordinated to three imidazoles and an OH group with the heme iron in the ferryl oxidation state coordinated to an imidazole as the fifth axial ligand and an unsubstituted porphyrin. Adding a Cl^- anion (restrained at the area where propionates used to be), Cu_B again moves toward the Fe=O moiety (Fe−Cu_B distance change from 4.19 to 3.97 Å), while it moves away upon substitution of Cl^- by a Na^+ cation (3.97 → 4.19 Å) or the absence of any ion next to the porphyrin (4.19 Å). Calculated heme-Fe/Cu_B distance deviations are of course constrained by the fixed atoms based on the QM/MM calculation but in any case demonstrate the Cu_B movement, if not quantitatively, qualitatively. Evaluation of the Hessian and calculation of the vibrational frequencies for these models shows a coupling between ν(Fe=O) and imidazole breathing in the cases where a Cl^- ion is present, at 722, 744, and 820 cm^{-1}, and in the absence of an ion at 703 and 804 cm^{-1}. The structure with the Na^+ ion exhibits ν(Fe=O) vibrational frequency with strong Fe=O stretching character at 824 cm^{-1}, but no resonances are observed.

In model **III**, we implemented an unsubstituted porphyrin at the ferryl-oxo oxidation state with an imidazole as the fifth axial ligand of heme-iron and a movable positive point charge (0.75+) on the N(His411)-Fe=O axis above ferryl oxygen. A graphical representation of the various frequencies for the Fe=O stretching, proximal imidazole breathing, and His411-Fe=O bending

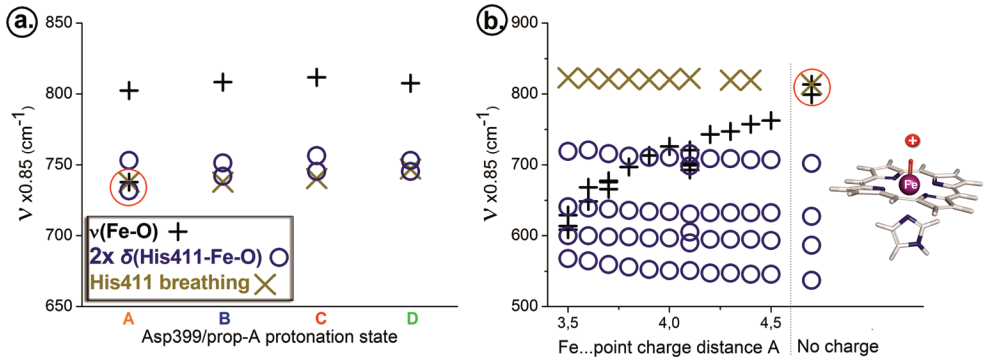

Figure 3. (a) Graph depicting the relative position of ν(Fe═O) stretching (+), Imidazole (His411) (×) breathing, and the δ(His411-Fe═O) multiplied by two bending vibrations (○) for the QM/MM systems under study in the protonation cases **A**, **B**, **C**, and **D**. All frequencies are scaled by the factor 0.85 to reproduce experimental values. The red circle indicates that the Fe═O stretching, Imidazole (His411) breathing, and δ(His411-Fe═O) bending frequencies are in near 1:1:2 resonance conditions. (b) Graph depicting the relative position of ν(Fe═O) stretching, Imidazole (His411) breathing, and δ(His411-Fe═O) multiplied by two bending vibrations for a small porphyrin model (model III) in the oxo-ferryl oxidation state including a movable positive charge of value 0.75+ above the imidazole-Fe═O moiety. All frequencies are scaled by the factor 0.85 to reproduce experimental values. The red circle indicates that Fe═O stretching and Imidazole breathing are to near resonance when the positive charge is absent. No 1:2 imidazole breathing:δ(His-Fe═O) bending resonance is observed here, in any of the studied models.

is shown in Figure 3b, with the latter multiplied by two. The 0.75+ point charge value was chosen based on the ESP-calculated charge on Cu_B in the QM/MM models. This model **III** group of structures manifests in the highest degree the sensitivity of ν(Fe═O) vibrational frequency by electrostatic interactions. The underlying anharmonicity in Fe═O stretching has also been previously reported using periodic orbits.[12]

Periodic orbit analysis in the active site of CcO (95 atoms) revealed one of the vibrational modes that include high amplitude Fe═O motions (f139 in Figure 3 of ref 12), as well as an imidazole breathing component, to develop a center-saddle bifurcation[49] by increasing the energy of the system and its frequency approaching the frequency of the vibrational mode f134 which is attributed to the imidazole breathing mode of His411.

In both graphs of Figure 3, while we observe negligible shifting for the imidazole breathing or δ(imidazole-Fe═O) bending vibrations, the ν(Fe═O) seems to be affected by protonation/deprotonation events in the area of prop-A. As can be clearly seen from Figure 3b, depending on the electrostatic environment near porphyrin, ν(Fe═O) is decoupled or tends to be coupled to the imidazole breathing vibration. It happens that coupling occurs when the positive point charge 0.75+ is absent. Isotopic difference ν(Fe═$^{16-18}$O) theoretical spectra calculated by MD methodology with models containing significantly fewer atoms as well as no solvent[12] show that protonation case **A** exerts a lower frequency peak at 799 cm^{-1} approaching the 773 cm^{-1} breathing vibrational frequency of imidazole, which seems to be stable and uninfluenced by nearby protonation events.

The effect of a positive charge, along the N(His411)-Fe═O axis, on the ν(Fe═O), can vary in its trend. In our theoretical models, the effect comes from either Cu_B on the protein QM/MM system (Figure 3a) or just a positive point charge of 0.75+ on the smaller DFT models (Figure 3b). For the protein models (QM/MM), as Cu_B gets further away from the heme-Fe, ν(Fe═O) is lowered by coupling to the imidazole breathing. For the smaller models, it is upshifting, when the point charge gets further away from the Fe═O unit, for the same coupling to occur (Figure 3b). Nevertheless, in both cases, a resonance does occur at some point. In the resonance effect proposed, we cannot exclude the involvement of the −OH group bound to Cu_B, as it can affect the overall charge of the Cu_B site sensed by the Fe═O moiety. We cannot exclude the case where the Cu_B−OH unit could exert a hydrogen-bonding interaction with the ferryl oxygen: stronger as it approaches the heme-iron or weaker as it gets further away. We have to note, though, that experimental data do not support the direct involvement of the −OH group in shifting ν(Fe═O) vibrational frequencies by H-bonding interactions.[21] In that study, the authors indicate a slight effect on the 804 cm^{-1} mode, as H/D exchange shifts ν(Fe═O) by only 2 cm^{-1}.

To account for the Cu_B−OH overall charge (<+0.75) effect, or even the effect of the coordinating Histidines, we repeated calculations based on model **III**, but with point charges of +0.25, −0.25, and the extreme case of −0.74. While for the +0.75 point charge models (**III**) the ν(Fe═O) varies in the 609−813 cm^{-1} range (Figure 3b), under the same configurations, point charge +0.25 gives ν(Fe═O) peaks between 774 and 790 cm^{-1}. Point charge −0.25 couples ν(Fe═O) to imidazole breathing in the range of 800−813 cm^{-1}, irrespective of the distance from the Fe^{IV}═O moiety. At the extreme case of a −0.74 point charge, ν(Fe═O) varies between 744 and 808 cm^{-1} and is coupled to imidazole breathing at large distances, greater than 4.0 Å, from the heme-Fe. In all the above cases of DFT models, imidazole breathing becomes higher or coupled (1:1 under −0.25 charge) in energy compared to ν(Fe═O). The most pronounced effect is exerted only on ν(Fe═O) by the +0.75 positive point charge on the His-Fe^{IV}═O axis. As charge sensed by the His-Fe^{IV}═O moiety lowers, even to extreme negative values (−0.74), the effect is reduced. This might be due to electrostatic interactions with the negative charge observed on ferryl oxygen.

Comparison between QM/MM Protein and DFT Active Site Models. The ν(Fe═O) stretching frequency comes higher in energy compared to the His411/Imidazole (CD2−NE2−CE1) breathing for the QM/MM optimized system (Figure 3a), while it comes lower for the smaller DFT models (Figure 3b). We should note that the proximal sides of the models giving rise to the graphs in Figures 3a and b are significantly different, in such a way that the proximal region is identified as the main contributor in regulating ν(Fe═O) energy to appear either higher or lower compared to the His411/Imidazole breathing. In this consensus, comparing different enzymatic systems[2−5] from *bovine*, *P. denitrificans*, or *Thermus thermophilus*, diversity in the proximal area can also control the coupling between Fe═O stretching and His411-Fe═O bending. This can also lead to diversity for the ν(Fe═O) stretching characteristics or behavior in the RR vibrational spectra.

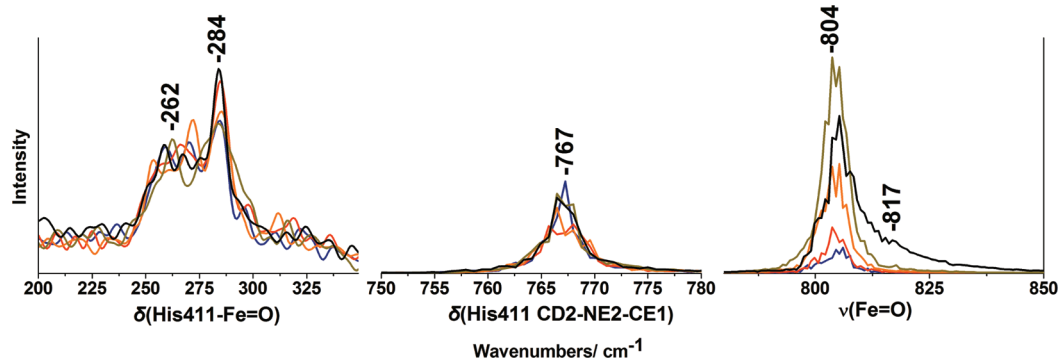

Figure 4. Power spectra derived by fast Fourier transforming the (a) His411-Fe=O angle, (b) CD2−NE2−CE1 (His411) angle, and (c) Fe=O distance time series of 43.5 ps trajectories in an NVE ensemble (0.5 fs time step) for the **A** protonation case of the heme a_3 ring A propionate/Asp399 pair. The curves correspond to averaging over twenty 43.5 ps long trajectories: at equilibrium (blue) and at Fe=O initial bond stretching enhancements to 1.8 (red), 2.0 (orange), 2.2 (dark green), and 2.5 Å (black line).

The proximal area of CcO enzymes consists of a hydrogen bonding network to proximal Histidine.[2−5] In the case of aa_3 oxidase from *bovine*[4] or *P. denitrificans*, Gly and Thr residues are present, while for the ba_3 from the *Thermus thermophilus* enzyme,[5] two Gly residues are only present. In each case, carbonyl groups act as O-donors to the hydrogen bonding network with varying strength. This should affect the relatively sensitive couplings occurring in His-Fe=O vibrations or in the course of the reaction with O_2 or H_2O_2 upon which one would expect conformational changes in the proximal area. The experimental vibrational spectra should reflect these conformational differences. In fact, in the experiments of oxygenated-MV mammalian aa_3, only one ferryl-oxo mode at 804 cm^{-1} is observed,[17,50] while both (790/804 cm^{-1}) can appear in others (see Table 1 and refs herein for details). Fe−N(His) modes would be less affected, as electron density from polarizing the N_δ−H bond of the proximal His would mainly move to the antibonding orbitals of the Fe^{IV}=O unit.

For the QM/MM optimized protein complex (Figures 2 and 3a), the δ(His411-Fe=O) bending vibration appears at a frequency half that of the His411 (Imidazole) breathing or Fe=O stretching modes, implying the 1:1:2 resonance. QM/MM calculations suggest that in the case of the protein models Cu_B has to move away from the heme a_3 group for the stretching/breathing/bending resonance to occur. We propose this Cu_B movement to be an on/off "switch" for the bending vibration to be active, as energy is added to the system, by laser excitation, enhancing the Fe=O stretching modes. This resonance does not occur in the smaller DFT models (Figure 3b).

Cu_B Effect. Turning our interest to the movement of Cu_B toward the heme-iron and thus closer to the ligand oxygen in the CcO/O_2 reaction, we propose that such a movement could be capable of changing redox equilibria, as the catalytic cycle of CcO is advancing, enabling Cu_B to inject electrons to the substrate. Such a mechanism would imply an interesting coupling between electron transfer and proton pumping activity, involving the prop-A/Asp399 pair which alters the Cu_B position and electron transfer from Cu_B or even the heme-Fe group. It is remarkable that enzymatic systems exhibit control points (switches) in such a way that vibrational couplings control a delicate equilibrium. For example, the change in the proximal environment (His411) comparing protein QM/MM and smaller active site models is adequate to reverse the $\nu(Fe^{IV}=O)$/δ(His411 CD2-NE2-CE1) relative energies. Such a delicate equilibrium should contain the proton−electron transfer coupling. Further investigations to identify such a link are underway in our lab.

C. Molecular Dynamics Calculations. In Figure 4, the power spectra from the MD calculations for protonation case **A** structure starting with an Fe=O bond distance of 1.67 Å (equilibrium) and elongated Fe=O stretching initial distances of 1.8, 2.0, 2.2, and 2.5 Å show an enhancement of the bending intensities at the 250−300 cm^{-1} region. Two peaks are mainly visible at 263 and 284 cm^{-1} in the lower spectral region. These peaks are related to His-Fe=O bending with the lower one to include an out-of-plane heme a_3 distortion, consistent with the two peaks depicted on the power spectrum from the MD simulation of a 95-atom active site system in our previous study[12] and on the QM/MM results previously reported in this study. Geometrical parameters such as distances, angles, and dihedrals for the Fe=O bond, His411-Fe=O group, and Cu_B site were based on QM/MM optimized structures reported herein, and we implemented an empirical potential (OPLS2005) without further tweaking it in order to not deviate a lot from its established parametrization. In consequence, the MD simulated spectra exert a shift for the bending vibration, compared to the experimental or QM/MM results. Nevertheless, even in this case, we observe coupling between the vibrations of the His411-Fe^{IV}=O unit.

For the 1.8, 2.0, and 2.2 Å (Figure 4) initial vibrational enhancement of the Fe=O stretching, we recorded an increase in the intensity of Fe=O stretching and His411-Fe=O bending modes, with the 284 cm^{-1} bending peak being enhanced. For the 2.5 Å Fe=O initial distance case, the spectrum differs again exhibiting an increase in the intensity of the 284 cm^{-1} bending peak but a decrease in that of the ν(Fe=O). For all above cases, a broad peak at the 500−600 cm^{-1} region is observed in the δ(His411-Fe^{IV}=O) spectrum (region not shown) which is also enhanced in intensity, indicating a rather broad range of induced enhancements in the His-(porphyrin)Fe^{IV}=O moiety. QM/MM derived frequencies in the 500−600 cm^{-1} region include porphyrin vibrations. The black line spectrum (Figure 4), although the highest amount of energy has been added to the system, exhibits peaks around 800 cm^{-1} with lower intensities compared to the previous enhancement at 2.2 Å (dark green spectrum). In contrast, the bending region is always increased in intensity. By differing excitation wavelengths, we can enhance the 340−360 cm^{-1} (bending) region along with a decrease of the intensities at the 750−810 cm^{-1} (stretching) region. Energy added to the His-(porphyrin)Fe^{IV}=O system seems to influence the intensities of several peaks including the His411-Fe=O bending, as well as that of the imidazole breathing vibration.

The imidazole breathing vibration, observed at 767 cm^{-1}, seems to have lost intensity as we initially enhanced Fe=O bond

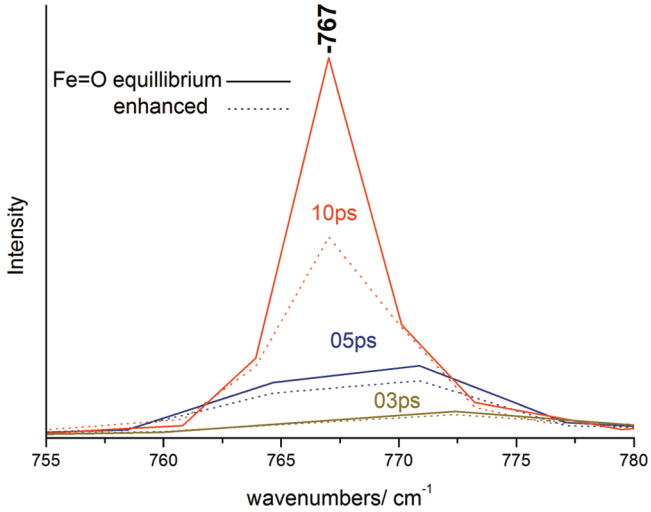

Figure 5. Power spectra derived by fast Fourier transforming the CD2−NE2−CE1 (His411) angle time series of 3 (green), 5 (blue), and 10 ps (red) trajectories in an NVE ensemble (0.5 fs time step) for the **A** protonation case of the heme a_3 ring A propionate/Asp399 pair. The curves correspond: at equilibrium (solid line) and immediately after the Fe═O initial bond stretching enhancement to 1.8 (dashed line).

stretching. In Figure 5, the time evolution of the 767 cm^{-1} peak is depicted for the equilibrium 1.67 Å (solid lines) and Fe═O stretching intensity enhancement at 1.8 Å (dashed lines) and integration times of 3, 5, and 10 ps. Intensity differences between equilibrium state 1.67 Å and enhanced Fe═O stretching at 1.8 Å become larger as time evolves. The intensity drop of the imidazole breathing mode (His411), as energy is added to the His-(porphyrin)-Fe═O system, coincides with the fact that this breathing mode is not shown in any experimental difference $^{16}O-^{18}O$ RR spectra of the ferryl intermediate.[16,21,50] In QM/MM results, for protonation case **A**, imidazole breathing is also shifted by the ^{18}O isotopic substitution, and thus it should be visible on a $^{16}O-^{18}O$ difference spectrum. In fact, this is not the case, as MD results show a suppression of imidazole breathing intensity, as the His-(porphyrin)Fe^{IV}═O system is excited.

Experiment and Theory. An equilibrium state of the CcO enzyme would be expected to be a **B** or **D** structure, with only one proton being shared between the heme a_3 ring A propionate and the adjacent Asp399 residue. Protonation states **A** or **C** would be expected to appear as transient species that can only be probed in a time-resolved experimental technique.[13,16,20,21,51] A steady-state experiment can most probably probe the equilibrium **B**- or **D**-based conformations.[23] In fact, we do not find the 1:1:2 resonance for the structures **B** or **D** (equilibrium) but only for **A** (transient) between the Fe═O stretching and the His411-Fe═O bending vibrations on the QM/MM level, consistent with the experimental results, where bending is not active in steady-state experiments. As these vibrations and consequently their couplings seem to be highly influenced by the electrostatic field sensed, it is most probable that a major factor, apart from the proton pumping in the time-resolved experiment, is the pH of the buffer in a steady-state experimental technique. Although we have demonstrated the Fe═O/imidazole breathing/His411-Fe═O resonance for the **A** case protein model only on the QM/MM level of theory, we propose that it represents and can be achieved with a rather broad range of protonation/deprotonation events near the active site of CcO. These events would all affect ν(Fe═O), but the mechanism remains essentially the same, and the prop-A/Asp399 pair is a highly qualified candidate for this process, as it is also involved in proton-pumping activity.[13−15]

It has previously been suggested that proton pumping activity in an enzyme is essential for the bending His411-Fe^{IV}═O vibration to be visible on the vibrational spectra.[52] Proton movement, including the deprotonation/protonation of the prop-A/Asp399 pair, induces a Cu_B movement toward or away from the heme a_3 group (QM/MM results). Even in the oxidized enzyme (ferryl intermediate), we observed a variation in the Fe−Cu_B distance to be between 3.8 and 4.3 Å, consistent with the trend in ref 53. For the protein QM/MM models, when Cu_B swings away from the heme a_3 group (no negative charges on the prop-A/Asp399 pair), Fe═O stretching and His411-Fe═O bending vibrations become highly coupled, thus both visible on the spectra. In this case, the relative intensities of Fe═O stretching and His411-Fe═O bending are based on the initial Fe^{IV}═O bond stretching enhancement (Figure 4). Thus, for the δ(His411-Fe═O) to be enhanced, we need low pH in a steady state, a short probing time, and an excitation wavelength adequate to strongly enhance initially the Fe^{IV}═O bond stretching and then lead to a suppressed $\nu(Fe^{IV}═O)$ intensity (like in the 2.5 Å initial stretching enhancement case). This is a rather qualitative and not quantitative study, as empirical MD spectra could not provide further quantitative details. A combination of the above parameters increases the chance for the bending to appear with the maximum intensity relatively higher than that of the Fe^{IV}═O stretching mode. Observation of the 356 cm^{-1} bending vibration in resonance Raman (RR) spectra depends highly on the excitation wavelength used: excitation at 441.6 or 413.1 nm enhances only the 800 cm^{-1} region, while excitations at 427.1, 426.8, 423.0, and 416.1 nm enhance both the 800 and 350 cm^{-1} spectral regions.[16,21,50] Interestingly, Oda et al.[21] have reported that the transition from the 571 cm^{-1} species (by the first electron reduced intermediate oxy $Fe^{III}-O-O-$) to the ferryl 804/356 cm^{-1} (Fe^{IV}═O) at pH 6.8 is significantly faster than that at pH 8.0, indicating also a pH dependence for the 356 cm^{-1} His411-Fe^{IV}═O bending vibration.

Table 2 summarizes the theoretical results reported in this study along with the experimental relative vibrational modes for the ferryl intermediates found in the literature and reported in detail in Table 1. During the **P** → **F** transition, a proton is released to the P side of the inner mitochondrial membrane indicating a proton movement in the CcO enzyme upon catalytic cycle.[54] It has become evident that the **P** intermediate is the $2e^-$ reduced ferryl-oxo species, while the **F** is the $3e^-$ reduced one.[23,25] Heme a^{2+} to a^{3+} oxidation, leading to the **F** intermediate, could affect the adjacent prop-A/Asp399 area of heme a_3 for the proton translocation to occur. On the basis of the current theoretical study, it is intriguing to propose that **P** → **F** transition induces conformational changes in the active site of the enzyme. This is possible by changing Fe−Cu_B distance as a consequence to proton translocation in the prop-A/Asp399 pair involved in proton pumping/translocation activity. In addition, while in the vibrational RR spectra of the **P** intermediate, the δ(His-Fe═O) bending mode appears at 356 cm^{-1}, such a mode is not present for the **F** intermediate. This comes in agreement with our theoretical results herein suggesting that the proton movement can alter vibrational resonances in the His-Fe═O unit, switching on or off the enhancement of the δ(His-Fe═O) bending mode.

IV. Conclusions

The QM/MM, MD, and DFT studies reported herein probe the vibrational spectroscopic properties of the His-Fe^{IV}═O unit in the oxo-ferryl oxidation state of CcO. We identify crucial resonances,

and we link them to conformational/structural changes during enzymatic turnover. Such a thorough and detailed study at the atomistic level helps to interpret experimental vibrational spectra. A clear link between peaks in a RR spectrum and the atomistic description of the CcO enzyme is a crucial step in clarifying its mechanism of action, while redox metal behavior is crucial to be structurally probed during enzymatic turnover. In the current theoretical study, we identify a displacement of the Cu_B metal in the oxo-ferryl species of the CcO + O_2 reaction due to protonation/deprotonation events in the matrix. Such a displacement controls the occurrence of a multiple stretching/breathing/bending 1:1:2 resonance in the His-Fe^{IV}═O moiety in the RR vibrational spectra. An eligible candidate for the cause of the displacement is the prop-A/Asp399 pair involved in proton pumping activity or motion in general during enzymatic turnover. The efficiency of the enhancement of the His-Fe═O bending vibration in the RR spectra is also controlled by the proximal Histidine hydrogen bonding networks, which are capable of altering the imidazole (His) breathing vibration. We propose that the bending vibration, δ(His−Fe^{IV}═O), can be significantly enhanced in the RR spectra, accompanied by a decrease in the intensity of the ν(Fe═O) stretching vibrations. The latter depends on the excitation wavelength in RR probing of the transient oxo-ferryl species (case **A**). As it seems that the position of Cu_B closer to or away from the heme a_3 plane is sensitive to protonation/deprotonation events in the enzyme, it can also occur during the **P** → **F** transition, where a proton is pumped by CcO. The heme a_3 prop-A/Asp399 pair may present a crucial switch for proton/electron coupling in CcO, as protonation states of the pair induce the reported heme a_3−Fe−Cu_B distance change. We expect that such a change in the heme a_3−Fe−Cu_B distance would also influence the O−O bond strength, in an intermediate like peroxy, and weaken it at the cleavage level (case a) or change the Fe═O bond strength (case b), making both intermediates (in cases a and b) vulnerable for a subsequent electron and proton transfer to yield the ferryl (heme a_3 Fe^{IV}═O/Cu_B−OH) and hydroxyl intermediates (heme a_3 Fe^{III}−OH/Cu_B−OH), respectively.

Acknowledgment. This research was financially supported by the European Union ToK grant GRID-COMPCHEM (MTKD-CT-2005-029583) and by a grant from the Spanish Ministry of Education and Science (to V.G.) through Project CTQ2007-62122/BQU. V.D. is grateful to Prof. Victor Guallar and to his research group for their hospitality, help, and valuable discussions on the QM/MM, MD, and DFT calculations in the Barcelona Supercomputing Center (BSC).

References and Notes

(1) Wikstrom, M. K. F. *Nature* **1977**, *266*, 271–273.
(2) Iwata, S.; Ostermeier, C.; Ludwig, B.; Michel, H. *Nature* **1995**, *376*, 660–669.
(3) Ostermeier, C.; Harrenga, A.; Ermler, U.; Michel, H. *Proc. Natl. Acad. Sci. U.S.A.* **1997**, *94*, 10547–10553.
(4) Tsukihara, T.; Aoyama, H.; Yamashita, E.; Tomizaki, T.; Yamaguchi, H.; Shinzawa-Itoh, K.; Nakashima, R.; Yaono, R.; Yoshikawa, S. *Science* **1996**, *272*, 1136–1144.
(5) Hunsicker-Wang, L. M.; Pacoma, R. L.; Chen, Y.; Fee, J. A.; Stout, C. D. *Acta Crystallogr., Sec. D* **2005**, *61*, 340–343.
(6) Ferguson-Miller, S.; Babcock, G. T. *Chem. Rev.* **1996**, *96*, 2889–2908.
(7) Michel, H.; Behr, J.; Harrenga, A.; Kannt, A. *Ann. Rev. Biophys. Biomol. Struct.* **1998**, *27*, 329–356.
(8) Belevich, I.; Verkhovsky, M. I. *Antioxid. Redox Signaling* **2008**, *10*, 1–30.
(9) Babcock, G. T.; Wikstrom, M. *Nature* **1992**, *356*, 301–309.
(10) Varotsis, C.; Babcock, G. T. *Biochemistry* **1990**, *29*, 7357–7362.
(11) Varotsis, C.; Zhang, Y.; Appelman, E. H.; Babcock, G. T. *Proc. Natl. Acad. Sci. U.S.A.* **1993**, *90*, 237–241.
(12) Daskalakis, V.; Farantos, S. C.; Varotsis, C. *J. Am. Chem. Soc.* **2008**, *130*, 12385–12393.
(13) Koutsoupakis, C.; Soulimane, T.; Varotsis, C. *J. Biol. Chem.* **2004**, *86*, 2438–2444.
(14) Pfitzner, U.; Hoffmeier, K.; Harrenga, A.; Kannt, A.; Michel, H.; Bamberg, E.; Richter, O.-M. H.; Ludwig, B. *Biochemistry* **2000**, *39*, 6756–6762.
(15) Koutsoupakis, C.; Pinakoulaki, E.; Stavrakis, S.; Daskalakis, V.; Varotsis, C. *Biochim. Biophys. Acta* **2004**, *1655*, 347–352.
(16) Han, S.; Takahashi, S.; Rousseau, D. L. *J. Biol. Chem.* **2000**, *275*, 1910–1919.
(17) Proshlyakov, D. A.; Pressler, M. A.; Babcock, G. T. *Proc. Natl. Acad. Sci. U.S.A.* **1998**, *95*, 8020–8025.
(18) Ogura, T.; Hirota, S.; Proshlyakov, D. A.; Shinzawa-Itoh, K.; Yoshikawa, S.; Kitagawa, T. *J. Am. Chem. Soc.* **1996**, *118*, 5443–5449.
(19) Kozlowski, P. M.; Kuta, J.; Ohta, T.; Kitagawa, T. *J. Inorg. Biochem.* **2006**, *100*, 744–750.
(20) Ogura, T.; Takahashi, S.; Shinzawa-Itoh, K.; Yoshikawa, S.; Kitagawa, T. *Bull. Chem. Soc. Jpn.* **1991**, *64*, 2901–2907.
(21) Oda, K.; Ogura, T.; Appelman, E. H.; Yoshikawa, S. *FEBS Lett.* **2004**, *570*, 161–165.
(22) Kitagawa, T.; Ogura, T. *Prog. Inorg. Chem.* **1997**, *45*, 431–479.
(23) Pinakoulaki, E.; Pfitzner, U.; Ludwig, B.; Varotsis, C. *J. Biol. Chem.* **2003**, *278*, 18761–18766.
(24) Proshlyakov, D. A.; Ogura, T.; Shinzawa-Itoh, K.; Yoshikawa, S.; Kitagawa, T. *Biochemistry* **1996**, *35*, 76–82.
(25) Proshlyakov, D.; Ogura, T.; Shinzawa-Itoh, K.; Yoshikawa, S.; Appelman, E.; Kitagawa, T. *J. Biol. Chem.* **1994**, *269*, 29385–29388.
(26) Ghosh, A.; Skancke, A. *J. Phys. Chem. B* **1998**, *102*, 10087–10090.
(27) Friesner, R. A.; Guallar, V. *Annu. Rev. Phys. Chem.* **2005**, *56*, 389–427.
(28) Fabian, M.; Palmer, G. *Biochemistry* **1999**, *38*, 6270–6275.
(29) Musatov, A.; Hebert, E.; Carroll, C. A.; Weintraub, S. T.; Robinson, N. C. *Biochemistry* **2004**, *43*, 1003–1009.
(30) Sucheta, A.; Georgiadis, K. E.; Einarsdottir, O. *Biochemistry* **1997**, *36*, 554–565.
(31) Szundi, I.; Liao, G.-L.; Einarsdottir, O. *Biochemistry* **2001**, *40*, 2332–2339.
(32) Siletsky, S.; Kaulen, A. D.; Konstantinov, A. A. *Biochemistry* **1999**, *38*, 4853–4861.
(33) Karpefors, M.; Adelroth, P.; Brzezinski, P. *Biochemistry* **2000**, *39*, 5045–5050.
(34) Kaila, V. R. I.; Verkhovsky, M. I.; Hummer, G.; Wikstrom, M. r. *Proc. Natl. Acad. Sci. U.S.A.* **2008**, *105*, 6255–6259.
(35) Nyquist, R. M.; Heitbrink, D.; Bolwien, C.; Gennis, R. B.; Heberle, J. *Proc. Natl. Acad. Sci. U.S.A.* **2003**, *100*, 8715–8720.
(36) Virginia Tech, http://biophysics.cs.vt.edu/H++.
(37) Jorgensen, W. L.; Tirado-Rives, J. *Proc. Natl. Acad. Sci. U.S.A.* **2005**, *102*, 6665–6670.
(38) Jorgensen, W. L.; Maxwell, D. S.; Tirado-Rives, J. *J. Am. Chem. Soc.* **1996**, *118*, 11225–11236.
(39) Jorgensen, W. L.; Tirado-Rives, J. *J. Am. Chem. Soc.* **1988**, *110*, 1657–1666.
(40) Jorgensen, W. L.; Chandrasekhar, J.; Madura, J. D.; Impey, R. W.; Klein, M. L. *J. Chem. Phys.* **1983**, *79*, 926–935.
(41) Schrodinger; 2008, http://www.schrodinger.com.
(42) *Desmond User manual*, Revision A; September 2008, http://www.schrodinger.com.
(43) *QSite User Guide*, Revision A, September 2008, http://www.schrodinger.com.
(44) Dunning, H. T., Jr.; Hay, P. J. *Modern. Theoretical Chemistry*; Plenum: New York, 1976; Vol. 3.
(45) Hay, P. J.; Wadt, W. R. *J. Chem. Phys.* **1985**, *82*, 270–283.
(46) Wadt, W. R.; Hay, P. J. *J. Chem. Phys.* **1985**, *82*, 284–298.
(47) Hay, P. J.; Wadt, W. R. *J. Chem. Phys.* **1985**, *82*, 299–310.
(48) Pople, J.; Scott, A.; Wong, M.; L., R. *Isr. J. Chem.* **1993**, *33*, 345–350.
(49) Farantos, S. C. *J. Chem. Phys.* **2007**, *126*, 175101–175107.
(50) Kim, Y.; Shinzawa-Itoh, K.; Yoshikawa, S.; Kitagawa, T. *J. Am. Chem. Soc.* **2001**, *123*, 757–758.
(51) Koutsoupakis, K.; Stavrakis, S.; Pinakoulaki, E.; Soulimane, T.; Varotsis, C. *J. Biol. Chem.* **2002**, *277*, 32860–32866.
(52) Kitagawa, T.; Ogura, T. *J. Bioenerg. Biomembr.* **1998**, *30*, 71–79.
(53) Qin, L.; Liu, J.; Mills, D.; Proshlyakov, D. A.; Hiser, C.; Ferguson-Miller, S. *Biochemistry* **2009**, *48*, 5121–5130.
(54) Belevich, I.; Verkhovsky, M. I.; Wikstrom, M. *Nature* **2006**, *440*, 829–832.

JP910006K